5

Modification of Carbon Nanofibres for Immobilisation of Metal Complexes. A Case Study with Rhodium-Anthranilic Acid

Abstract

The immobilisation of the rhodium-anthranilic acid complex onto fishbone carbon nanofibres was executed via the following steps: (i) surface oxidation of the fibres, (ii) conversion of the carboxyl groups into acid chloride groups, (iii) attachment of anthranilic acid and (iv) complexation of rhodium by the attached anthranilic acid. The immobilisation process was followed and the resulting surface species were characterised by IR, XPS, XAFS spectroscopy, and molecular modelling. Anthranilic acid bonds to the CNFs by an amide linkage with the carboxyl groups that are present after surface oxidation of the fibres. The immobilised anthranilic acid co-ordinates to rhodium via the nitrogen atom and the carboxyl group. The as-synthesised Rh(III) complex itself is not active in the liquid-phase hydrogenation of cyclohexene. After reduction with sodium borohydride in order to obtain a Rh(I) complex, small (d = 1.5-2 nm) rhodium metal particles result, which are highly active. The results indicate that different activation procedures for the immobilised Rh/anthranilic acid system should be applied, such as reduction with a milder reduction agent or direct complexation of the rhodium in the Rh(I) state.

5.1 Introduction

The immobilisation of homogeneous catalysts onto solid supports has been studied extensively since the 1970s.[1-4] The objective is to combine the advantages of homogeneous catalysts, such as a high selectivity and metal efficiency, with an easy recovery of the catalyst. A number of immobilisation methods can be distinguished, such as encapsulation or entrapment, supported liquid phase, and immobilisation by covalent bonding.

In general, immobilisation by covalent bonding ('immobilisation') of homogeneous hydrogenation catalysts is executed by first attaching one ligand to the support. This ligand is usually the most important ligand, for example, a bulky bidentate ligand that causes the immobilised catalyst to be enantioselective. Next, the metal complex is co-ordinated to the immobilised ligand by a ligand exchange reaction. Other immobilisation procedures are used as well, such as reaction of a metal salt with the immobilised ligand, which may be followed by a further co-ordination of other ligands to the metal atom, and direct reaction of the metal centre with a surface atom of the support. Most immobilisation techniques try to maintain the structure of the immobilised catalyst as close as possible to that of its homogeneous precursor. The first 15 years of research into immobilisation have learned that simply immobilising a successful homogeneously active metal complex catalyst to a functionalised support mostly yields an inferior version of the homogeneous catalyst.[2] However, it has also been shown that by careful design supported metal complex catalysts can be prepared that have advantages not exhibited in homogeneous catalysis. Although some of the immobilised metal complex catalysts have properties that are as good or even better than their homogeneous counterparts, in 1998 none had an industrial application.[4] This is correlated to the frequent observation of significant metal leaching, although other important factors, such as the mechanical and macroscopic properties of the support are decisive too. The problem of leaching is often directly related to the mechanism of the catalytic reaction. For instance, immobilised phosphine-containing metal complexes will leach under hydrogenation conditions, because during catalysis one phosphine ligand must desorb to allow the required co-ordination of the olefin. This problem can sometimes be circumvented by using multidentate ligands.

An alternative approach could be to purposely change the electronic and steric features of the complex by immobilisation. This approach has been exemplified by Holy, who studied the immobilisation of rhodium N-phenyl anthranilic acid (RhPAA) and rhodium anthranilic acid (RhAA) onto polystyrene.[5-7] Figure 5.1 shows the structure of N-phenyl anthranilic acid and anthranilic acid. The DMF-soluble Rh(I) complex of PAA was known as a remarkably active hydrogenation catalyst.[8-11] However, upon immobilisation onto polystyrene the catalyst did not display any activity. In contrast, when anthranilic acid was immobilised, a highly active Rh(I) catalyst was obtained after reduction of the metal complex with

$NaBH_4$. Monovalent rhodium is able to undergo the oxidative addition-reductive elimination cycle that is needed for catalysing hydrogenation reactions. The rhodium-anthranilic acid complex was not known as a homogeneous catalyst. In addition, the immobilised complex of anthranilic acid with nickel showed hydrogenation activity.[12] This example demonstrates that the catalytic properties of immobilised complexes often differ from that of the non-supported counterparts. It could, therefore, be the best approach to design immobilised catalysts that do not have homogeneous analogues. A weak ligand in solution, e.g., an amine ligand, which may easily dissociate from the metal resulting in reduction of the metal under hydrogenation conditions, could be a suitable ligand for an immobilised system.

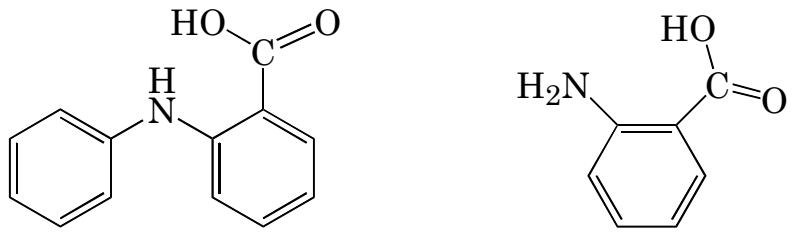

PAA AA

Figure 5.1 Structure of N-phenyl anthranilic acid (PAA) and anthranilic acid (AA).

Although the Rh/anthranilic acid complex has been successfully immobilised on polystyrene, the relatively low thermal and mechanical stability, the swelling properties and the microporous structure of the polystyrene support complicate the use of the catalyst in an industrial environment. Carbon nanofibres (CNFs), on the other hand, are mechanically very strong and have a macroporous structure. The hydrophobicity of the fibres can be modified by surface oxidation.[13] Furthermore, the CNFs obtained after synthesis are very pure and can be grown at low cost.[14] These advantages cause the CNFs to be a suitable support for catalytic reactions in the liquid phase. Consequently, we decided to immobilise RhAA onto fishbone type carbon nanofibres.

As yet the immobilisation (i.e., by covalent bonding) of metal complexes onto carbon nanofibres or carbon nanotubes has, to our best knowledge, not been explored. Some reports describe the impregnation or adsorption of homogeneous catalysts on these new carbon materials.[15-17] Moreover, only few articles have been published about the immobilisation of metal complexes on carbon in general. Kagan *et al.*[18] synthesised a chiral rhodium catalyst on partially graphitised carbon, while McCabe and Orchin[19] attached cobalt and tin complexes to bituminous coal. The inertness of CNFs and, to a lesser extent, of carbon in general makes immobilisation with these materials much more difficult

than with polymers or oxidic supports, such as silica or alumina. However, already in the 1970s Miller and co-workers[20] modified graphite electrodes for the attachment of amines on their surface. The electrodes were kept at high temperature in air, the resulting carboxyl groups were converted into acid chloride groups by the action of thionyl chloride, and these groups were subsequently reacted with an amine. The approach of Miller has been used by several other researchers for the attachment of molecules or even metal-ligand systems to carbon electrodes, although the experimental conditions for oxidation and attachment of amine varied considerably.[21-24] Smalley and co-workers[25] and, more importantly, Haddon and co-workers.[26, 27] employed the method of conversion of carboxyl groups on carbons to acid chloride groups and subsequent attachment of amines to shortened single-walled carbon nanotubes (SWNTs). Haddon *et al.* used this procedure to solubilise the SWNTs by bonding of long-chain organic molecules to its surface. Raw SWNTs were oxidised and shortened by prolonged sonication in a mixture of nitric and sulfuric acid. The carboxyl groups, which were presumably positioned at the edges of the tubes of a length of 300 nm, were converted to acid chloride groups by refluxing in thionyl chloride [containing some N,N-dimethylformamide (DMF)] for 24 hrs. The DMF acts as a catalyst in the formation of acid chloride groups by $SOCl_2$.[28] Haddon *et al.* emphasised that reaction of the $SOCl_2$-treated SWNTs with octadecylamine (ODA) in toluene was unsuccessful. The key to the preparation was the reaction of the tubes with pure molten ODA for an extended period of time. It is obvious that severe reaction conditions are required for derivatisation of carbon nanomaterials.

In this investigation we have studied the immobilisation of the rhodium-anthranilic acid complex onto fishbone carbon nanofibres. The reports by Haddon and co-workers and by Holy served as a basis to develop an immobilisation scheme. It will be shown that the Rh(III)/anthranilic acid system immobilised on carbon nanofibres can indeed be synthesised. The complex is bonded to the fibres by an amide linkage of the CNF carboxyl groups and the amine functionality of anthranilic acid. The immobilised Rh(III) complex is not active in the hydrogenation of cyclohexene. Upon reduction with $NaBH_4$, a very active catalyst consisting of extremely small rhodium metal particles results. Milder activation procedures may lead to an active immobilised Rh(I) complex.

5.2 Experimental

5.2.1 Growth of fishbone carbon nanofibres

Carbon nanofibres of the fishbone type were produced by catalytic decomposition of CH_4 on a Ni/Al_2O_3 catalyst.[29-32]

The Ni/Al_2O_3 catalyst with 30 wt% Ni metal loading was synthesised by the deposition-precipitation technique.[33] Alumina (Alon-C, Degussa) was suspended in an acidified aqueous solution of nickel nitrate (Acros, 99 %) and diluted ammonia was injected within two hours at room temperature under vigorous stirring until the pH had reached a value of 8.5. After overnight stirring, the suspension was filtered, washed, and dried at 120°C. Finally, the catalyst was calcined at 600°C in stagnant air for three hours.

For the production of fishbone CNFs, 0.5 g of the 30 wt% Ni/Al_2O_3 catalyst was reduced at 600°C in 14 % H_2/N_2 (flow rate 350 ml/min) in a vertical tubular reactor (diameter 3 cm) for two hours. After having decreased the temperature to 570°C, methane (50 % in N_2, flow rate 450 ml/min) was passed through the catalyst bed for 6.5 hours. The yield of fibres amounted to approximately 12 g.

5.2.2 Immobilisation of Rh/anthranilic acid onto fishbone carbon nanofibres

Figure 5.2 represents schematically the experimental procedures used for the immobilisation of Rh/anthranilic acid onto fishbone CNFs. The carbon nanofibres were first oxidised in a mineral acid mixture in order to create carboxyl groups on the surface and to remove the original Ni/Al_2O_3 growth catalyst (1). These carboxyl groups were converted into acid chloride groups by the action of thionyl chloride and DMF (2). Anthranilic acid was bonded to the fibres by reaction with these acid chlorides (3). Subsequently, the immobilised anthranilic acid was complexed to rhodium by refluxing the fibres in an aqueous solution of rhodium(III) chloride (4). Finally, the Rh/anthranilic acid complex was reduced with sodium borohydride (procedure not shown in Figure 5.2). Steps 2 and 3 (generation of acid chloride groups and attachment of anthranilic acid) were carried out under a nitrogen atmosphere, using standard Schlenk techniques.

The fishbone carbon nanofibres were oxidised in a mixture of concentrated nitric and sulphuric acid. Five grams of CNFs were boiled under reflux in 80 ml HNO_3/H_2SO_4 1:1 for 30 min (HNO_3: Lamers & Pleugers, 65 %, pure; H_2SO_4: Merck, 95-97 %, p.a.). Upon cooling and dilution with demineralised water, the suspension was filtered over a Teflon membrane filter with a pore diameter of 0.2 μm, washed with demineralised water until the washings showed no significant acidity, and dried at 120°C for 16 hrs.

Three grams of oxidised fibres were treated with 50 ml $SOCl_2$/DMF 50:1 (DMF: N, N-dimethylformamide) by boiling under reflux for 24 hrs in a N_2 atmosphere ($SOCl_2$: Acros, 99.5+ %; DMF: Merck, p.a.). After cooling, the reaction mixture was decanted from the fibres, which were, subsequently, dried in vacuum at 40°C for five hours. Another batch of fibres was dried in vacuum for 17 hours at room temperature to make sure that all DMF was removed from the $SOCl_2$-treated fibres.

Twenty grams of anthranilic acid (Acros, 98+ %) were dried in vacuum at 40°C for two hours and transferred under N_2 to the $SOCl_2$-treated fibres. This mixture was kept at a temperature above the melting point of anthranilic acid (144-148°C) for 96 hrs. Upon cooling, the resulting purple liquid suspension was filtered over a Teflon membrane filter with a pore diameter of 0.2 μm, thoroughly washed with ethanol, and dried in vacuum at room temperature for 17 hours. In an additional experiment the $SOCl_2$-treated fibres were reacted with a solution of anthranilic acid in DMF. The fibres were boiled under reflux for 96 hrs in a 1 M solution of dried anthranilic acid in molsieve-dried DMF (20 ml). These fibres were washed with DMF and further treated identically.

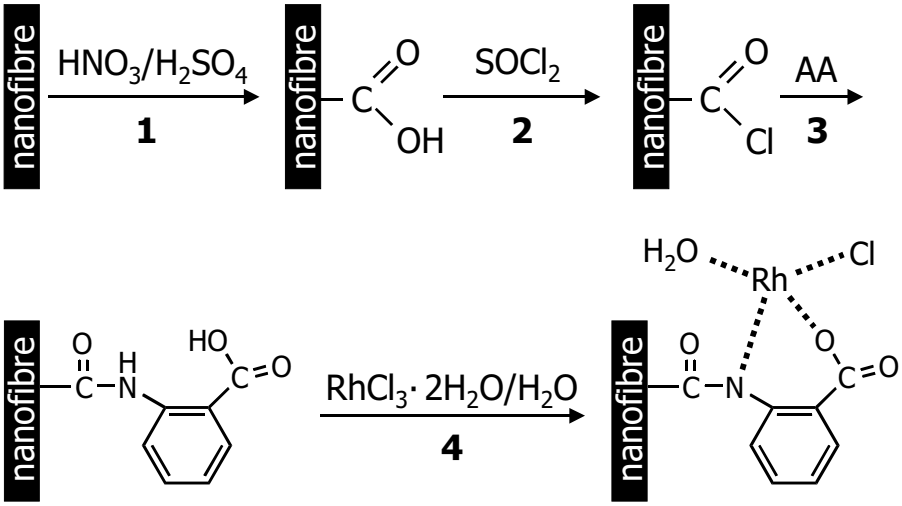

Figure 5.2 Schematic depiction of the experimental procedures used for the immobilisation of Rh/anthranilic acid on fishbone carbon nanofibres.

Two grams of anthranilic acid-reacted fibres were dispersed in 30 ml demineralised water, 48 mg $RhCl_3 \cdot 2H_2O$ (0.2 mmole) was added, and the suspension was boiled under reflux for 72 hours. Upon cooling, the Rh-loaded fibres (max. 1 wt%) were separated from the colourless water fraction by filtration, washed with demineralised water, and dried in vacuum at room temperature for 17 hours.

Reduction of the immobilised Rh/AA complex was carried out by dispersing one gram of Rh/AA/CNFs in 10 ml ethanol (Merck, p.a.) and by adding 55 mg

$NaBH_4$ (Alfa, 99 %) in 10 ml ethanol. The evolution of gas indicated an immediate reaction. After stirring for 30 minutes at room temperature, the reduced catalyst was filtered from the colourless solution, washed with ethanol, and dried in vacuum at room temperature for 17 hours.

Table 5.1 contains the codes of the intermediate products and the final immobilised catalysts.

Table 5.1 Codes for the intermediate products and the final immobilised catalysts.

Code	Description
Intermediate products	
CNF-U	Untreated fibres
CNF-OX	Oxidised fibres
CNF-$SOCl_2$	$SOCl_2$-treated fibres
CNF-AA	Anthranilic acid reacted fibres
Final catalysts	
RhAA/CNF(17)	Dried for 17 hrs after $SOCl_2$ treatment
RhAA/CNF(17, BH)	Dried for 17 hrs, reduction with $NaBH_4$
RhAA/CNF(5)	Dried for 5 hrs after $SOCl_2$ treatment
RhAA/CNF(17, DMF)	Dried for 17 hrs, reaction AA in DMF

5.2.3 Characterisation

Characterisation of the samples was carried out by infrared spectroscopy (IR), X-ray photoelectron spectroscopy (XPS), X-ray absorption fine structure (XAFS) spectroscopy, and molecular modelling.

Infrared spectroscopy

Transmission infrared spectra were recorded on a Perkin Elmer 2000 spectrometer equipped with an air dryer for removal of water vapour and carbon dioxide. One hundred scans were co-added at a resolution of 8 cm^{-1} and a boxcar apodisation. Samples were prepared by thoroughly mixing a small amount of ground nanofibres with pre-dried KBr. Tablets were pressed at 4 tons/cm^2 in vacuum for two minutes. The concentrations of the nanofibres ranged from 0.1 to 1 ‰ (m/m). All transmission spectra were baseline corrected.

X-ray photoelectron spectroscopy

The XPS data were obtained with a Vacuum Generators XPS system, using a CLAM-2 hemispherical analyser for electron detection. Non-monochromatic

Al(K_α) X-ray radiation was utilised by employing an anode current of 20 mA at 10 keV. The pass energy of the analyser was set at 20 eV.

Due to the overlap of the Rh_{3d} signal with the broad C_{1s} peak, the C_{1s} signal of CNF-AA was subtracted from the C_{1s}/Rh_{3d} peak of the rhodium-loaded catalysts, resulting in the isolation of the Rh signal. It was ascertained that the error in the intensity of the subtracted spectrum at the position of the maximum of the C_{1s} peak was not more than the intensity of the Rh signal and that the baseline was exhibiting zero intensity after subtraction.

XAFS spectroscopy

XAFS data collection. XAFS spectra at the Rh K edge (23220 eV) were obtained at the HASYLAB (Hamburg, Germany) synchrotron beamline X1.1, which was equipped with a Si(311) double crystal monochromator. The monochromator was detuned to 50 % of the maximum intensity to minimise the presence of higher harmonics. All measurements were performed in the transmission mode using ionisation chambers filled with an Ar/N_2 mixture to have an absorbance of 20 and 80 % in the first and the second ionisation chamber, respectively.

The CNF-samples (300 mg) were pressed into self-supporting wafers and mounted into an *in situ* EXAFS cell equipped with Be windows.[34] Due to the low concentration of Rh (1 wt%), the calculated edge step was about 0.2. The Rh_2O_3 and $RhCl_3$ reference compounds (Aldrich, 99.8 % and 98 %, respectively) were diluted with boron nitride (Alfa, 99.8 %) and pressed into self-supporting wafers (calculated edge step 1). The rhodium reference foil (Aldrich, 99.9 %, 25 μm thickness) was mounted on the sample holder with Kapton tape. The EXAFS cell was flushed with purified He for 15 minutes and cooled down to liquid nitrogen temperature prior to measurement.

XAFS data-processing. Extraction of the EXAFS data from the measured absorption spectra was performed with the XDAP code developed by Vaarkamp *et al.*[35] Two or three scans were averaged and the pre-edge was subtracted using a modified Victoreen curve.[36] The background was subtracted employing cubic spline routines with a continuously adjustable smooth parameter.[37, 38] Normalisation was performed by dividing the data by the height of the absorption edge at 50 eV.

EXAFS phase-shifts and backscattering amplitudes. Data for phase shifts and backscattering amplitudes were obtained from the reference compounds: Rh foil for Rh-Rh, $RhCl_3$ for Rh-Cl, and Rh_2O_3 for Rh-O, Rh-C and Rh-N contributions.[38] Table 5.2 gives the crystallographic data and the forward and inverse Fourier transform ranges used to create the EXAFS references. Both the reference spectra and the samples were measured at liquid nitrogen temperature. This means that no temperature effect has to be included in the difference in Debye-

Waller factor ($\Delta\sigma^2$) between sample and reference as obtained in the EXAFS data-analysis.

Table 5.2 Crystallographic data and the forward and inverse Fourier Transform ranges used to make the EXAFS references.

						Forward FT	Inverse FT
Atom pair	Ref compd	Ref	N^{ref}	R^{ref} (Å)	k^n	ΔK (Å^{-1})	ΔR (Å)
Rh-Rh	Rh foil	39	12	2.69	3	2.7-22.7	1.4-3.1
Rh-O	Rh_2O_3[a]	40	6	2.05	1	3.7-16.3	0.0-2.3
Rh-Cl	$RhCl_3$	41	6	2.30	1	3.1-18.0	0.0-2.9

[a] it was established with XRD that the Rh_2O_3 was in the hexagonal form.

R-space fitting, difference file technique and weight factor k^n. The EXAFS data-analysis program XDAP allows one to perform multiple-shell fitting in R-space by minimising the residuals between both the magnitude and the imaginary part of the Fourier transforms of the data and the fit. R-space fitting has important advantages compared to the usually applied fitting in k-space, and is extensively discussed in a recent paper by Koningsberger *et al.*[38]

The difference file technique was applied together with phase-corrected Fourier transforms to resolve the different contributions in the EXAFS data.[38] The difference file technique allows one to optimise each individual contribution with respect to the other contributions present in the EXAFS spectrum. If the experimental spectrum is composed of different contributions, then:

$$\text{Exp.Data} = \sum_{i=1}^{N} (\text{Fit})_i \,, \tag{5.1}$$

whereby $(\text{Fit})_i$ represents the fitted contribution of co-ordination shell *i*. For each individual contribution the following equation should then be valid:

$$(\text{Fit})_j = \text{Exp.Data} - \sum_{i=1 \text{ and } i \neq j}^{N} (\text{Fit})_i \tag{5.2}$$

The right-hand side of this equation is further denoted as the difference file of shell *j*. A good fit is only obtained if the total fit and each individual contributing co-ordination shell describe correctly the experimental EXAFS and the difference file, respectively. In this way, not only the total EXAFS fit, but also the individual fits of all separate contributions can be determined reliably.

Both high Z (e.g. Metal-Metal) and low Z (e.g. Metal-Oxygen) contributions may be present in the EXAFS data collected on metal complexes immobilised on supports of a high surface area. The low Z contributions may arise from the ligands and/or from the support. A k^3 weighting emphasises the high Z contributions to the spectrum, since high Z elements have more scattering power at high values of k than low Z elements. However, the use of a k^3 weighted EXAFS spectrum or Fourier transform makes the analysis much less sensitive to the presence of low Z contributions in the EXAFS data. In this study, the EXAFS fits have been checked by applying k^1, k^2 and k^3 weightings in order to be certain that the results are the same for all weightings.

Number of independent data points, variance and statistical significance. The number of independent data points (N_{indp}) was determined as outlined in the "Reports on Standard and Criteria in XAFS Spectroscopy":[42]

$$N_{indp} = \frac{2\Delta k \Delta R}{\pi} + 2 \tag{5.3}$$

The variances of the magnitude and imaginary part of the Fourier transforms of fit and data were calculated according:

$$\text{Variance} = \frac{\int \left[k^n \left(FT^n_{model}(R) - FT^n_{exp}(R) \right) \right]^2 dR}{\int \left[k^n FT^n_{exp}(R) \right]^2 dR} \times 100 \tag{5.4}$$

In this study the statistical significance of a contribution has been checked by a comparison of the amplitude of $(Fit)_j$ with the noise level present in the difference file (the noise in the difference file is essentially the same as the noise in the experimental data).

Molecular modelling

Molecular modelling was executed with the force-field based program Cerius[2]. The universal force-field routine was used. A (part of a) carbon nanofibre was simulated by taking several unit cells of graphite.

5.2.4 Catalytic test experiments

The catalytic activity of the immobilised Rh complexes in the hydrogenation of cyclohexene was tested in a semi-batch slurry reactor, operated at a constant pressure of 1200 mbar H_2. The thermostated, double-walled reaction vessel was equipped with vertical baffles and a gas-tight stirrer with a hollow shaft and blades for gas recirculation. The stirrer was operated at 2000 rpm. During reaction, the hydrogen consumption was automatically monitored by a mass flow meter. It was assured that, under the conditions used, the rate of dissolution of H_2 in the solvent was higher than the maximum measurable rate of H_2-uptake.

In a typical experiment, the reaction vessel was filled with 100 mg of catalyst and 100 ml of ethanol (Merck p.a.). Next, the reactor was thermostated at 25°C, evacuated, filled with H_2, and pressurised. The reaction was started by injection of 1 ml cyclohexene (Acros 99 %) with a syringe and was allowed to proceed until total hydrogenation of the cyclohexene.

5.3 Results

Infrared spectroscopy

Figure 5.3 shows the infrared spectra of CNF-U, CNF-OX, CNF-AA and of a physical mixture of carbon nanofibres and anthranilic acid. To allow comparison, transmission levels of all spectra were kept approximately the same. It was established that, within the transmission window used, the intensity of the bands did not depend upon the transmission level of the spectra. Table 5.3 summarises the band assignments. The assignment of the bands of untreated fibres and of oxidised fibres have been given and discussed in Chapter 2 and Chapter 3, respectively. Concerning the untreated fibres, the absorptions at about 1630 and at 1384 cm^{-1} are due to adsorbed water and nitrate on the KBr, respectively, and can be discounted.[43-46] The minimum at 1582 cm^{-1} originates from an aromatic ring vibration, while the broad 1200 cm^{-1} absorption is attributed to the C-C stretching vibration. [44, 47, 48] Upon oxidation, an additional band appears in the spectrum of the fibres at 1724 cm^{-1}. This peak originates from the C=O stretching vibration of carboxyl and/or carbonyl groups.[43, 44, 47, 49] Furthermore, the intensity of the 1200 cm^{-1} absorption intensifies due to CO stretching and OH bending vibrations, occurring in that region.[47] The intensity of the 1582 cm^{-1} band also increases, because, upon oxidation, symmetry restrictions are relieved for more aromatic rings.[50]

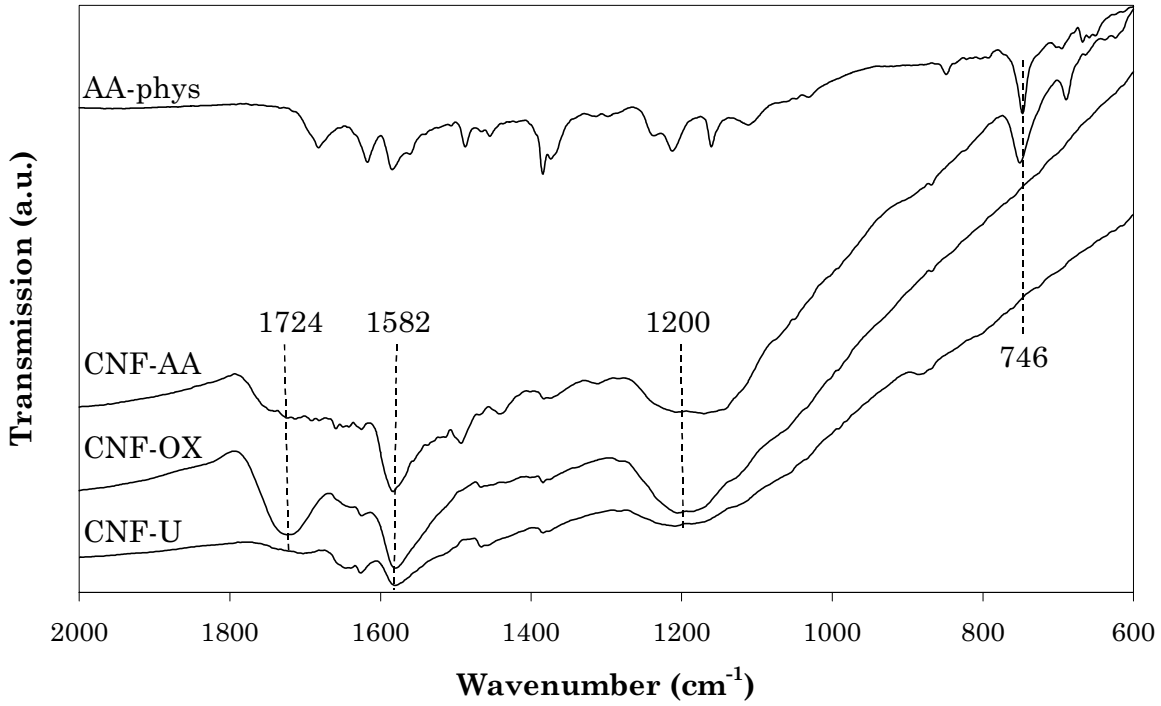

Figure 5.3 IR spectra of untreated (CNF-U), oxidised (CNF-OX), anthranilic acid reacted (CNF-AA) carbon nanofibres, and of a physical mixture of anthranilic acid and CNFs (AA phys).

Table 5.3 Assignments of infrared absorptions found for CNF-U, CNF-OX, CNF-AA and a physical mixture of CNFs and anthranilic acid.

Wavenumber (cm^{-1})	Assignment	Reference
1724	C=O stretching carbonyl & carboxyl	43, 44, 47, 49
1633	adsorbed water	43, 44
1582	aromatic ring stretching	44, 47, 48
1384	nitrate	45, 46
1200	C-C stretching	44, 47
746	aromatic C-H bending anthranilic acid	51

A comparison of the IR spectrum of a physical mixture of anthranilic acid and CNFs (AA-phys) with that of pure AA (not shown) indicates that due to the strong IR absorbance of CNFs many bands visible in the spectrum of pure AA diminish, shift or even disappear upon mixing with carbon nanofibres. Therefore, the aromatic C-H bending mode at 746 cm^{-1} (indicative for four adjacent H atoms[51]) occurring in the spectrum of CNF-AA appears to be the best indication

for the presence of anthranilic acid on the surface of the CNFs. Besides, other absorptions are visible in the spectrum of CNF-AA that can be attributed to anthranilic acid. Furthermore, in the spectrum of CNF-AA the carboxyl C=O stretching vibration at 1724 cm^{-1} of CNF-OX has almost disappeared, indicating that an amide bond between the carboxyl groups on the CNFs and the amine groups of anthranilic acid has been formed.

The spectrum of CNF-$SOCl_2$ (not shown) was identical to that of CNF-OX. The spectrum of the fibres that were treated with anthranilic acid in DMF showed only a weak band at 753 cm^{-1}. Furthermore, the C=O stretching vibration at 1724 cm^{-1} was only slightly diminished.

X-ray photoelectron spectroscopy

The process of immobilisation was followed with XPS as well. Figure 5.4 shows the Cl_{2p} (Fig. 5.4A) and the N_{1s} (Fig. 5.4B) region of CNF-OX, CNF-$SOCl_2$, CNF-AA, and RhAA/CNF(5). Oxidised fibres do not contain chlorine, but after treatment with $SOCl_2$ this element is clearly present. Upon reaction with anthranilic acid, the chlorine is removed, whereas after complexation of Rh (with $RhCl_3 \cdot 2H_2O$) it reappears on the surface of the CNFs. The presence of nitrogen on oxidised fibres is not detected with XPS. The small peak appearing in the spectrum of CNF-$SOCl_2$ can be attributed to small traces of DMF that is used during this synthesis step. The spectrum of CNF-$SOCl_2$ in Figure 5.4B has been obtained from CNF-$SOCl_2$ fibres that were dried only for five hours under vacuum. The CNF-AA fibres clearly contain nitrogen, which remains present

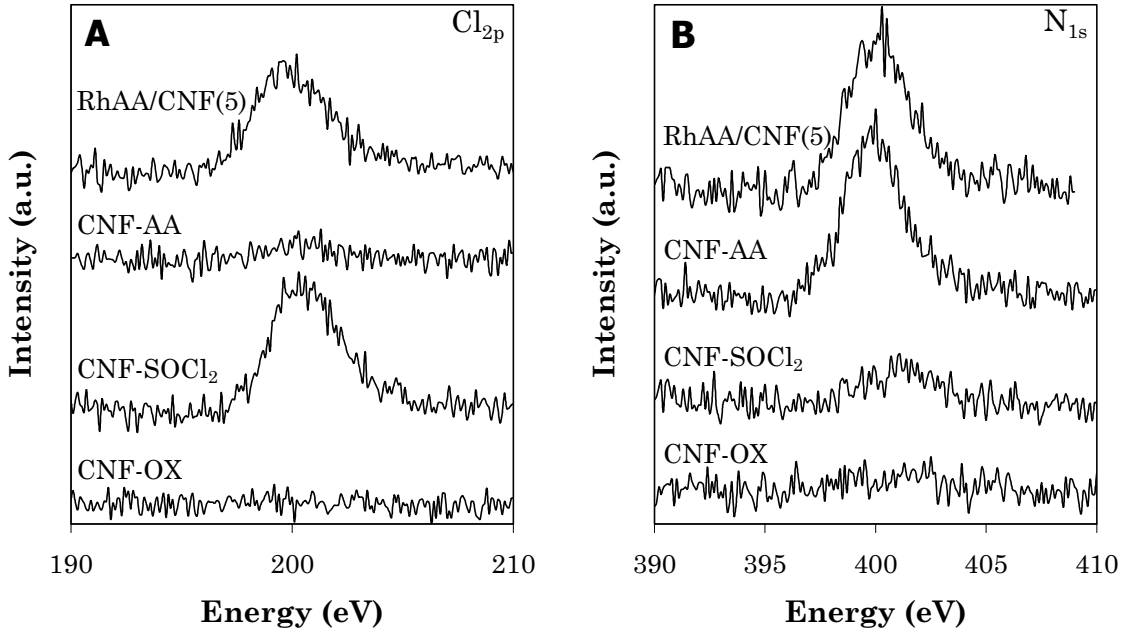

Figure 5.4 XPS spectra of A) the Cl_{2p} region and B) the N_{1s} region of CNF-OX, CNF-$SOCl_2$, CNF-AA, and RhAA/CNF(5).

after complexation of Rh. Reduction with $NaBH_4$ or catalytic reaction does not affect the intensity of the N_{1s} peak (spectra not shown).

The presence and the oxidation state of Rh was studied by monitoring the Rh_{3d} peak. Figure 5.5 displays the results. The $Rh_{3d5/2}$ and $Rh_{3d3/2}$ transitions are both clearly visible. Only the $Rh_{3d5/2}$ peaks were used for further analysis. The spectrum of RhAA/CNF(17) shows one broad $Rh_{3d5/2}$ peak centred at 308.9 eV. Literature values for the $Rh_{3d5/2}$ peak in Rh_2O_3 and $RhCl_3$ are 308.2-308.8 eV and 310.1 eV, respectively.[52] We can, therefore, conclude that the Rh is in the trivalent oxidation state in this complex. Upon reduction of the RhAA/CNF(17) complex with $NaBH_4$ (denoted as RhAA/CNF(17, BH)), a second peak at about 307.4 eV has become the most intense one and the peak at 308.9 eV is visible as a shoulder. As the $Rh_{3d5/2}$ peak for rhodium metal lies at 307.2 eV,[52] this new maximum indicates the presence of Rh(0). Clearly, a large part of the Rh is in the zerovalent state after reduction with $NaBH_4$. A Rh(I) complex would have given a peak at about 308 ev.[52]

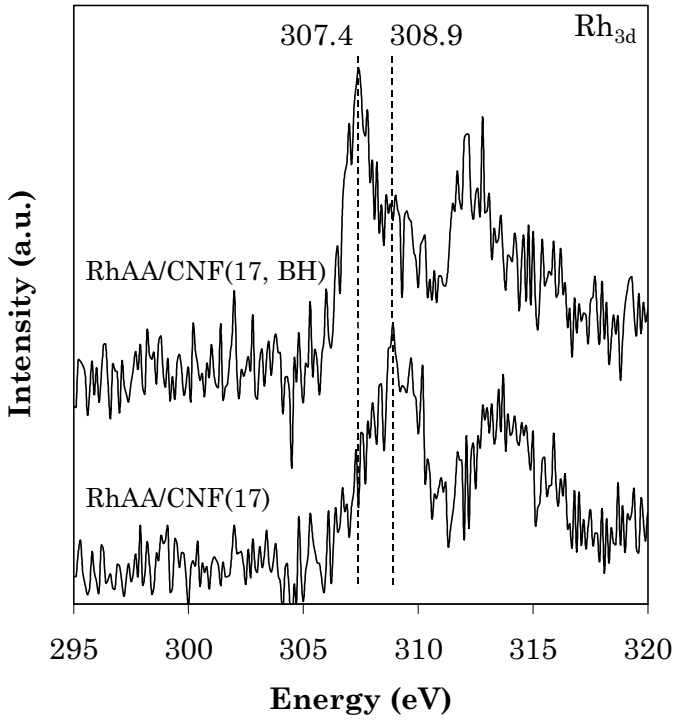

Figure 5.5 XPS spectra of the Rh_{3d} region of RhAA/CNF(17) and RhAA/CNF(17, BH).

XAFS spectroscopy

XANES. The X-ray absorption near edge spectra of RhAA/CNF(17) and RhAA/CNF(17, BH) are shown in Figure 5.6 together with the data for Rh-foil and Rh_2O_3. By comparison of the spectra of the RhAA/CNF(17) and RhAA/CNF(17, BH) samples with the reference compounds, information can be

obtained about the oxidation state of the rhodium. The absorption edge of RhAA/CNF(17) is almost identical to that of Rh_2O_3. Thus, we can conclude that the Rh in RhAA/CNF(17) is in the trivalent oxidation state. No Rh-Rh is present.

The position of the lower half of the absorption edge of RhAA/CNF(17, BH) is at a lower energy than that of RhAA/CNF(17) and closer to that of Rh-foil. The increase in absorption intensity in this region of the absorption edge is typical of zerovalent rhodium. This suggests that part of the rhodium is in the zerovalent oxidation state.

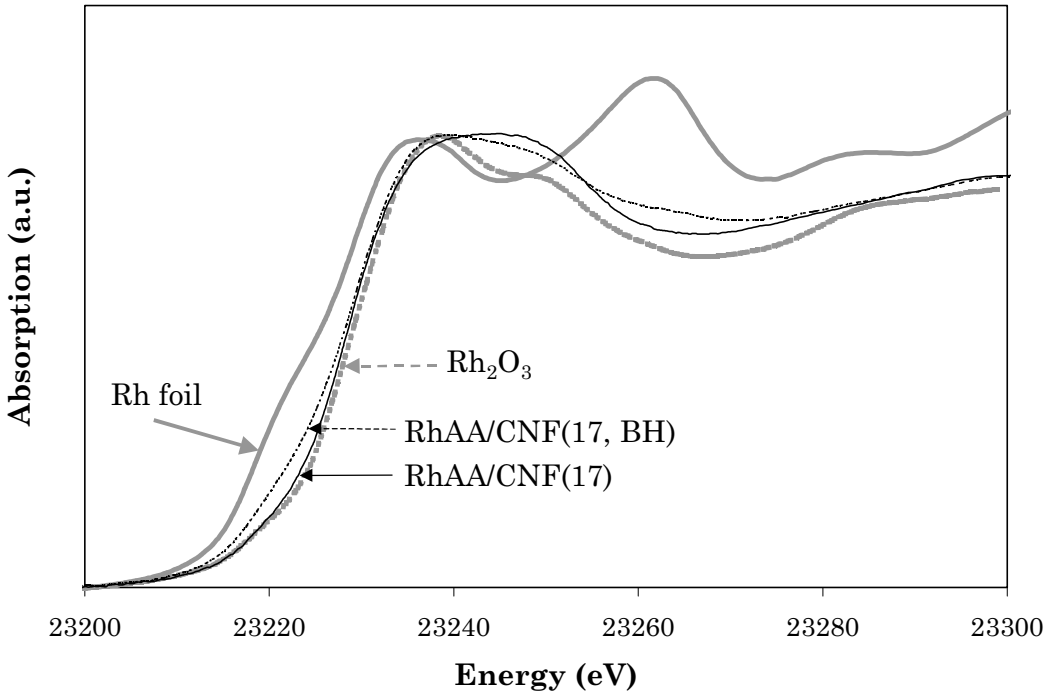

Figure 5.6 XANES spectra of RhAA/CNF(17) (solid black) and RhAA/CNF(17, BH) (dotted black) together with Rh foil (solid grey) and Rh_2O_3 (dotted grey).

EXAFS analysis. Figure 5.7 shows the experimental EXAFS data of RhAA/CNF(17) (Figure 5.7A) and RhAA/CNF(17, BH) (Figure 5.7C). The data quality is excellent. The signal-to-noise ratio at k = 4.4 $Å^{-1}$ amounts to approximately 150 for RhAA/CNF(17) and 75 for RhAA/CNF(17, BH). It can clearly be seen that the EXAFS intensity of sample RHAA/CNF(17, BH) at larger values of k (k > 10 $Å^{-1}$) is higher than for RhAA/CNF(17), indicating the presence of a high Z scatterer.[38] The k^2-Fourier transform of the EXAFS data of RhAA/CNF(17) and RhAA/CNF(17, BH) are displayed in Figure 5.7B and D, respectively. Whereas the peak at 1.6 Å in both samples originates from low Z scatterers, such as oxygen, the peak at 2.4 Å in the uncorrected Fourier transform of the EXAFS data of RhAA/CNF(17, BH) is due to a Rh-Rh

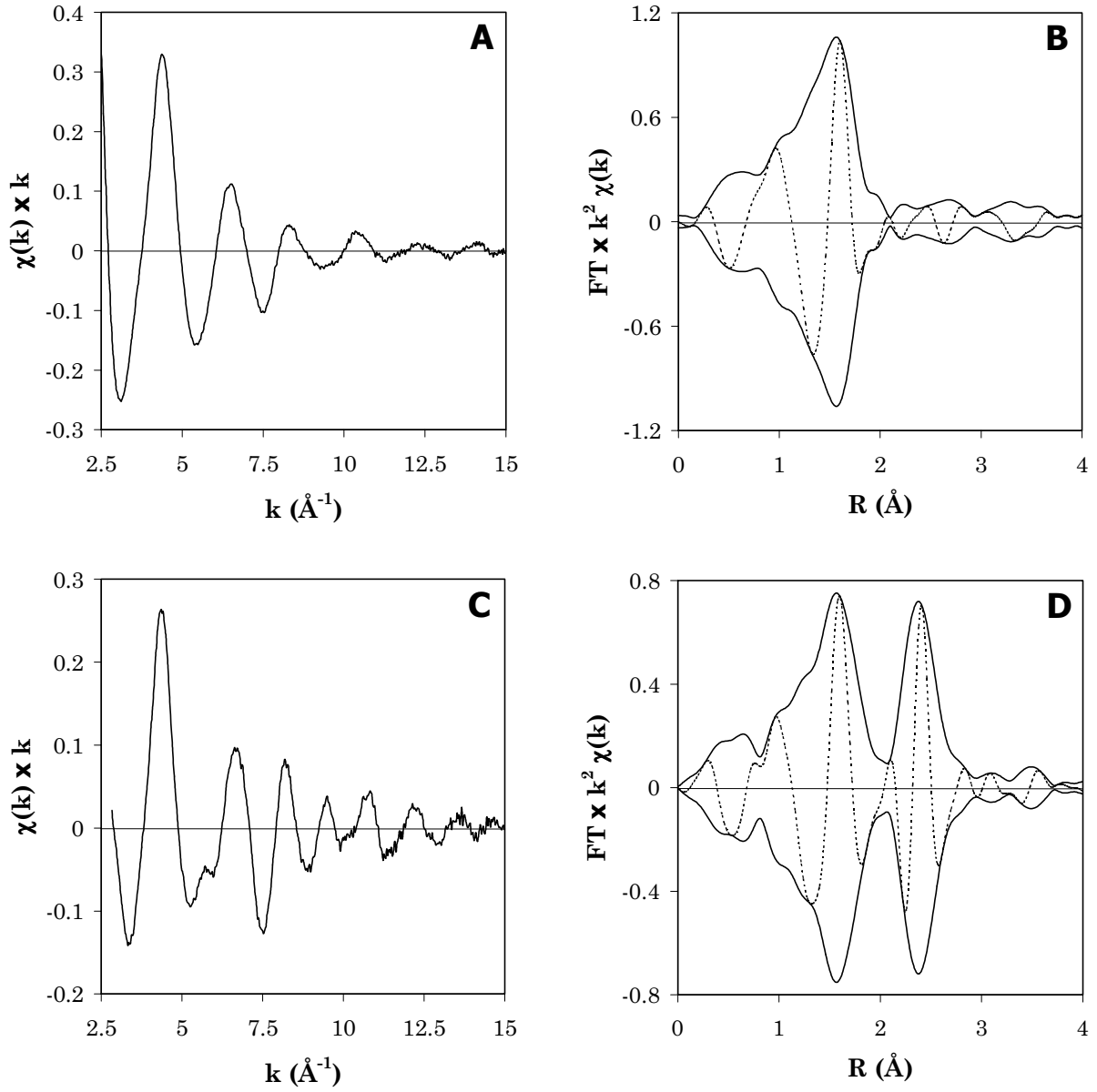

Figure 5.7 A) Experimental EXAFS spectrum of RhAA/CNF(17) (k^1 weighted)
B) Corresponding uncorrected Fourier transform (k^2 weighted, Δk = 2.7-15.9 $Å^{-1}$)
C) Experimental EXAFS spectrum of RhAA/CNF(17, BH) (k^1 weighted)
D) Corresponding uncorrected Fourier transform (k^2 weighted, Δk = 2.9-15.9 $Å^{-1}$).

contribution. Also, the intensity of the first shell region at 1.6 Å is lower, indicating a change in co-ordination after reduction.

Figure 5.8A shows the Fourier transform of the experimental EXAFS data of RhAA/CNF(17) together with the FT of the total fit. The fit quality is excellent for the used fit range (ΔR = 1-2.8 Å). In RhAA/CNF(17) Rh-O/N, Rh-Cl and Rh-C contributions could be determined. The phase-corrected Fourier transforms of the fits of each individual contribution together with their corresponding difference

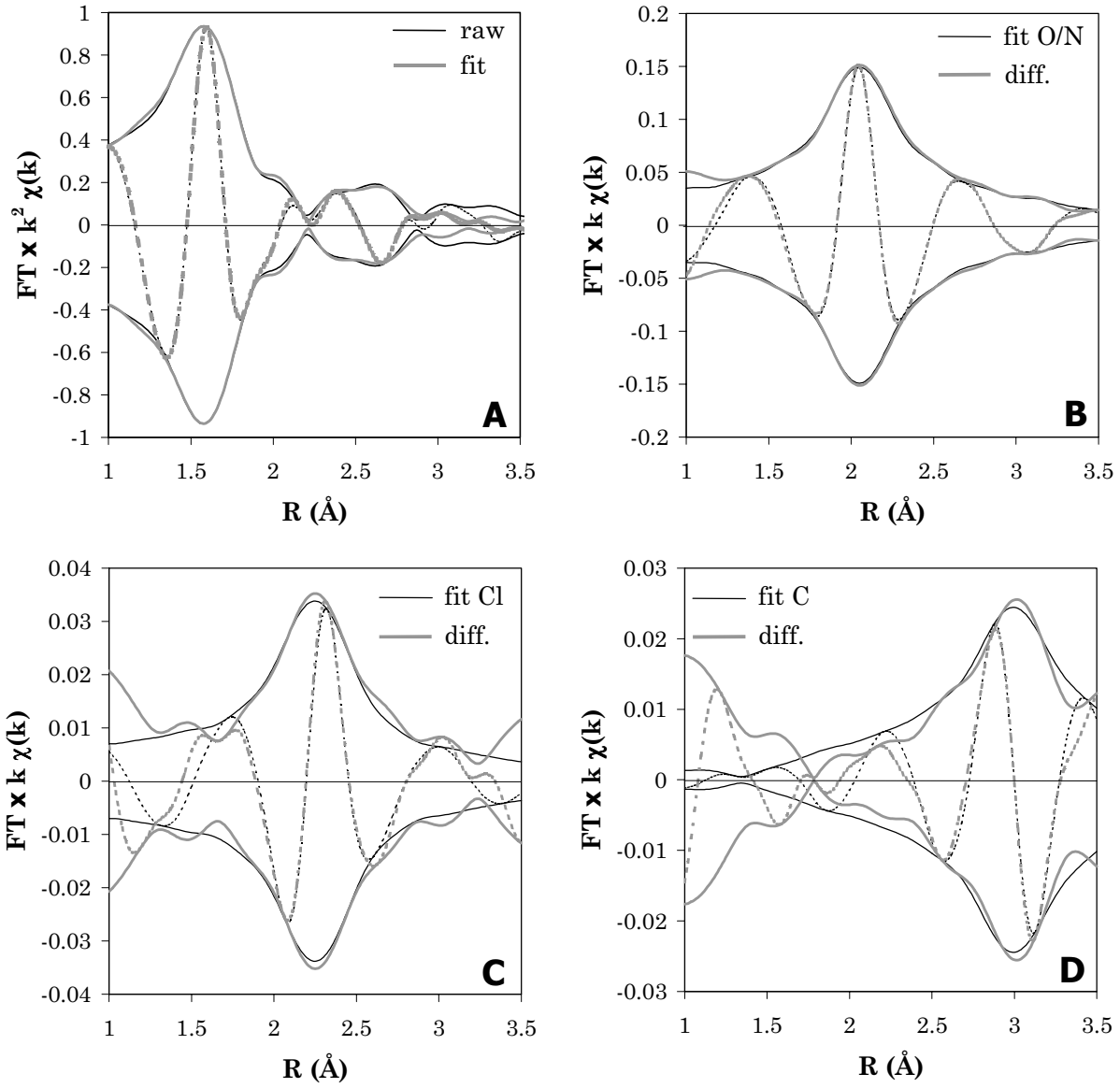

Figure 5.8 Fit results of RhAA/CNF(17) (Δk = 3.9-14 Å^{-1}, ΔR = 1-2.8 Å) A) Fourier transform of experimental EXAFS data and total fit (k^2 weighted, uncorrected) B) Rhodium-oxygen fit and corresponding difference file (k^1 weighted, Rh-O phase-corrected) C) Rhodium-chlorine fit and corresponding difference file (k^1 weighted, Rh-Cl phase-corrected) D) Rhodium-carbon fit and corresponding difference file (k^1 weighted, Rh-C phase-corrected).

files are shown in Fig. 5.8B, C, and D for the Rh-O/N, Rh-Cl, and Rh-C contributions, respectively. The fit quality of each individual contribution is very good, indicating that reliable fit results for the weaker EXAFS contributions have been obtained as well. Table 5.4 presents the fit parameters of the EXAFS spectra resulting from the multiple shell fits in R-space and the variances of the

imaginary and absolute part of the fits for all catalysts. All variances obtained are well below 1 %, indicating that excellent fit results for all catalysts have been acquired.[38] Furthermore, the calculated number of independent data points (see Equation 5.3) is 14, showing that a fit with three shells is possible (N_{indp} = 12). Because the contributions of carbon, oxygen or nitrogen in RhAA/CNF(17) cannot be easily distinguished, all these interactions were fitted with the Rh_2O_3 reference. The rhodium atom in the immobilised complex has five oxygen or nitrogen neighbours at a distance of 2.05 Å. The presence of carbon at such a distance is unlikely. One chlorine atom is also present in the co-ordination sphere of Rh at a distance of 2.28 Å. At a larger distance of 2.94 Å three neighbours are fitted, which are most likely carbon atoms. No Rh-Rh interactions could be fitted.

Table 5.4 Fit parameters of EXAFS spectra and variances of fits (Δk = 3.9-14 Å^{-1}, ΔR = 1-2.8 Å, k^2 weighted).

Catalyst	Atom	N	R (Å)	$\Delta\sigma^2$ (Å^2)	ΔE_0 (eV)	k^2-variance (%)	
		± 5 %	± 1 %	± 5 %	± 10 %	Im	Abs
RhAA/CNF(17)	O/N	5.0	2.05	0.001	-3.1	0.12	0.05
	Cl	1.0	2.28	0.004	4.4		
	C	2.9	2.94	0.003	-10.6		
RhAA/CNF(17, BH)	Rh	4.5	2.68	0.006	9.9	0.25	0.12
	O	3.4	2.05	0.001	-4.4		
	C	1.6	2.25	0.008	-8.6		
RhAA/CNF(5)	Rh	2.0	2.69	0.006	7.0	0.06	0.03
	O	4.1	2.07	0.006	-9.2		
	Cl	2.6	2.28	0.004	10.7		
RhAA/CNF(17, DMF)	Rh	8.2	2.69	0.000	5.6	0.10	0.04
	O	1.3	2.05	0.004	-8.5		

The fit results of RhAA/CNF(17, BH) are shown in Figure 5.9. Again, very good results are obtained for the total fit and the three separate Rh-Rh, Rh-O and Rh-C contributions. At a distance of 2.68 Å 4.5 Rh neighbours are situated (see Table 5.4). The co-ordination number of oxygen neighbours amounts to 3.4 at 2.05 Å. Finally, 1.6 carbon atoms are visible at a distance of 2.25 Å.

Figure 5.10 shows the experimental EXAFS data of RhAA/CNF(5) (Figure 5.10A) and RhAA/CNF(17, DMF) (Figure 5.10C). The signal-to-noise ratio at k = 4.4 Å^{-1} amounts to approximately 50 for RhAA/CNF(5) and 150 for RhAA/CNF(17, DMF). The spectrum of RhAA/CNF(5) is similar to that of

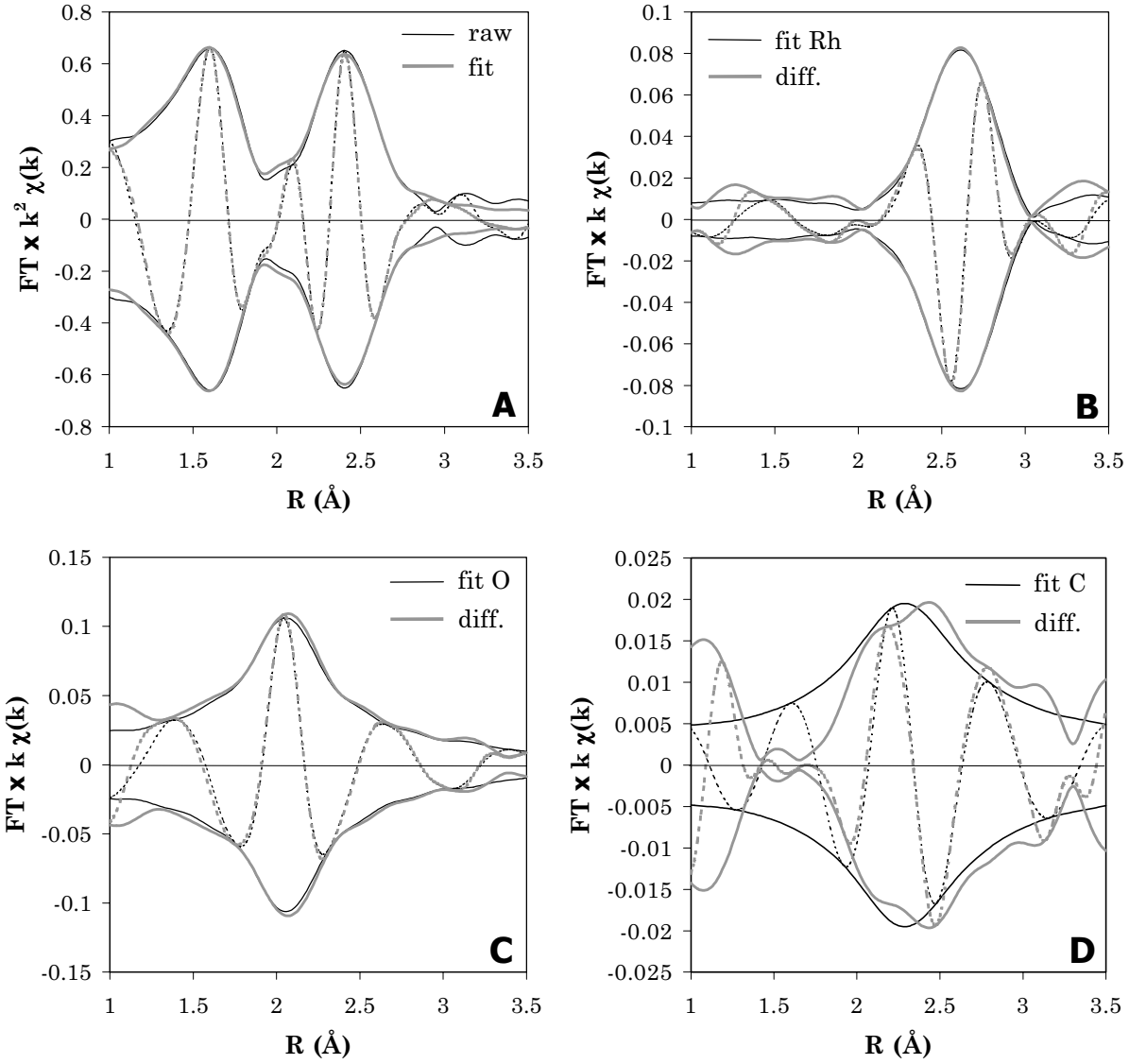

Figure 5.9 Fit results of RhAA/CNF(17, BH) (Δk = 3.9-14 Å^{-1}, ΔR = 1-2.8 Å) A) Fourier transform of experimental EXAFS data and total fit (k^2 weighted, uncorrected) B) Rhodium-rhodium fit and corresponding difference file (k^1 weighted, Rh-Rh phase-corrected) C) Rhodium-oxygen fit and corresponding difference file (k^1 weighted, Rh-O phase-corrected) D) Rhodium-carbon fit and corresponding difference file (k^1 weighted, Rh-C phase-corrected).

RhAA/CNF(17). However, at large k values (k > 10 Å^{-1}) a somewhat higher intensity is found, indicating the presence of Rh-Rh in this catalyst. This is supported by the peak at 2.4 Å in the uncorrected FT of the EXAFS data (Figure 5.10B). The EXAFS spectrum of RhAA/CNF(17, DMF) displays a much higher intensity up to large k values (k > 10 Å^{-1}), evidencing the presence of relatively

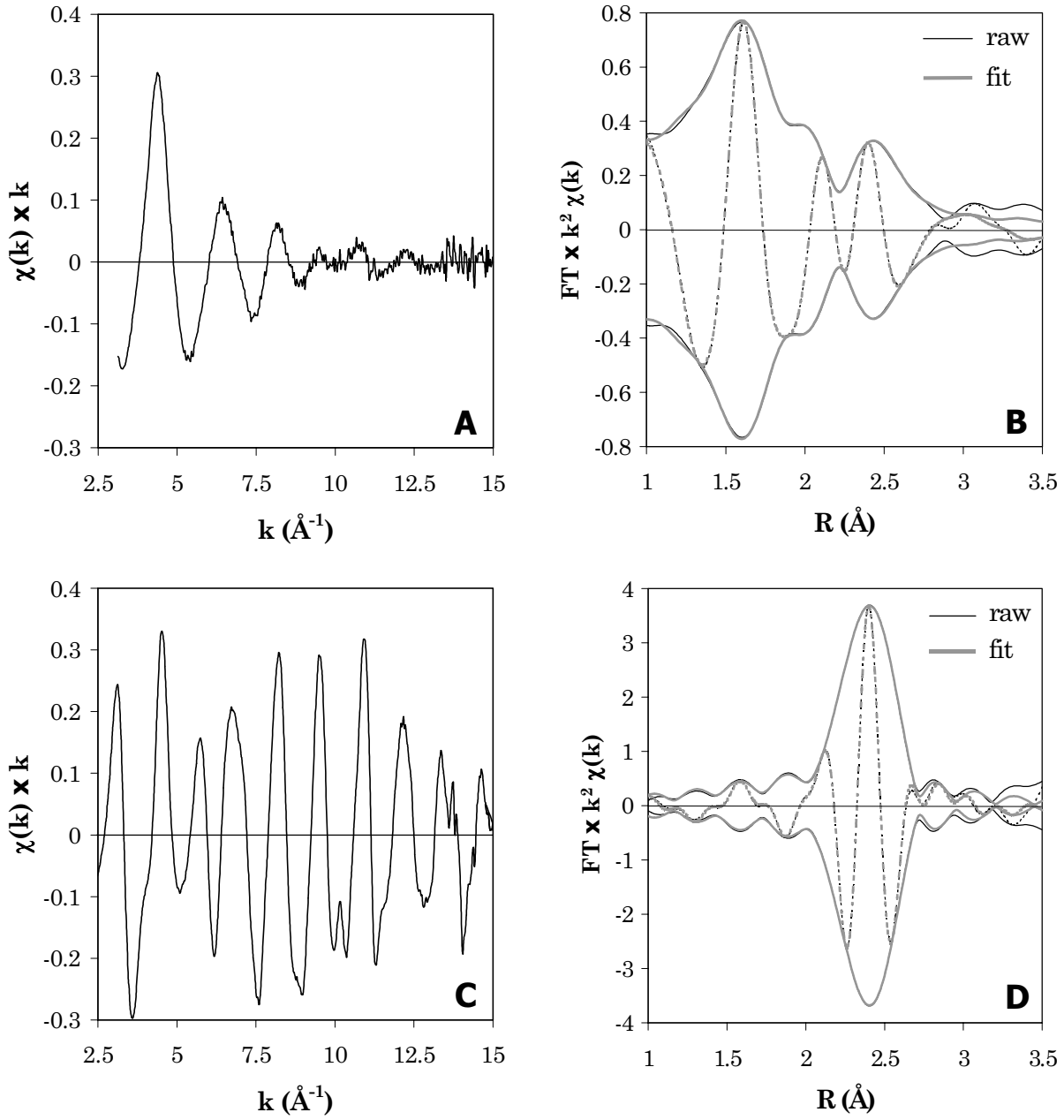

Figure 5.10 A) Experimental k^1 weighted EXAFS spectrum of RhAA/CNF(5) B) Corresponding uncorrected Fourier transform and total fit (Δk = 3.9-14 $Å^{-1}$, ΔR = 1-2.8 Å, k^2 weighted) C) Experimental k^1 weighted EXAFS spectrum of RhAA/CNF(17, DMF) D) Corresponding uncorrected Fourier transform and total fit (Δk = 3.9-16.3 $Å^{-1}$, ΔR = 1-2.8 Å, k^2 weighted).

large Rh particles. Indeed, the FT of the EXAFS data mainly displays a large peak at 2.4 Å. The fit parameters displayed in Table 5.4 show that, besides oxygen and chlorine contributions (N_O = 4.1, R_O = 2.07, N_{Cl} = 2.6, R_{Cl} = 2.28), RhAA/CNF(5) indeed contains some Rh-Rh (N = 2.0, R = 2.69). A reasonable fit

can also be obtained with less chlorine. RhAA/CNF(17, DMF) contains almost exclusively Rh-Rh (N = 8.2, R = 2.69). Some Rh-O is present as well (N = 1.3, R = 2.05).

It should be noted that with all catalysts edge steps were obtained that were equal to the theoretical edge step for 1 wt% Rh on carbon. In other words, all catalysts indeed contain 1 wt% of Rh. The total discoloration of the water phase (containing the equivalent of 1 wt% Rh) after complexation of rhodium supports these observations.

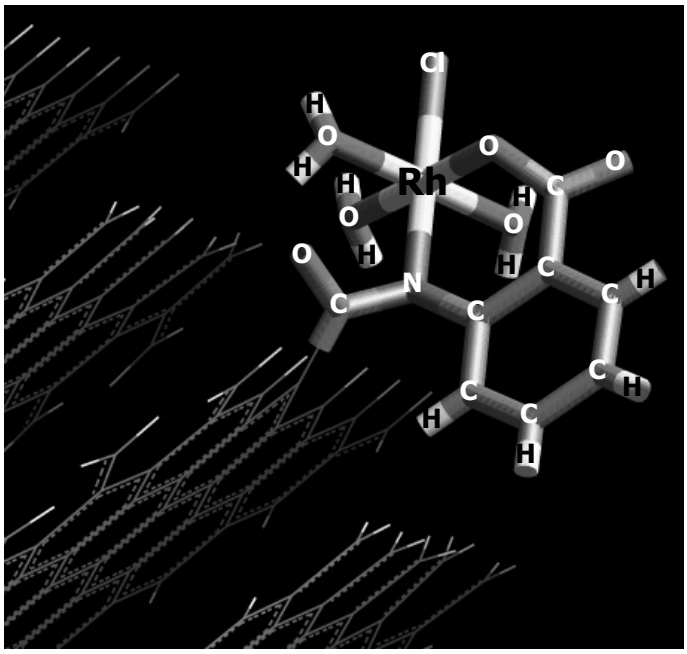

Figure 5.11 Outcome of the molecular modelling study of RhAA/CNF(17).

Molecular modelling

The outcome of the EXAFS fit results of RhAA/CNF(17), i.e., the number and nature of neighbours of Rh, were used as input for the molecular modelling study. It was assumed that the rhodium is in the trivalent oxidation state and that, for reasons of charge compensation, both the carboxyl and the amide group of anthranilic acid are ionised. The result is shown in Figure 5.11. On the left-hand side of the figure the carbon nanofibre structure is visible. Anthranilic acid is bonded to the fibre via an amide bond with a carboxyl group on the surface of the CNF. Rh is co-ordinated to anthranilic acid via one oxygen of the carboxyl group (of AA) and via the nitrogen atom. Besides one chloride anion, the co-ordination sphere of the rhodium atom is completed by three water molecules (the last synthesis step was performed in water). Thus, the Rh atom is octahedrally surrounded. Table 5.5 gives the distances of several atoms to the central Rh atom. For comparison, the EXAFS results have been included as well. The oxygen

atoms of the three water molecules are situated at a distance of 1.9 Å. The oxygen atom of the carboxyl group of anthranilic acid is found at 2.0 Å, as is the AA nitrogen atom. Chloride resides at a distance of 2.3 Å. Three carbon atoms are found at distances of 2.8 Å (C of carboxyl group AA), 3.0 Å (carbon of benzyl ring) and 3.0 Å (C of carboxyl group CNF). These distances agree very well with the EXAFS results.

Table 5.5 Distances between Rh and several atoms in the molecular model of RhAA/CNF(17). For comparison, the EXAFS results have been included.

	Modelling		EXAFS	
Atom	Nr of atoms	Distance (Å)	N	R (Å)
O_{H2O}	3	1.9 (3x)		
$O_{carb.}$	1	2.0	5.0	2.05
N	1	2.0		
Cl	1	2.3	1.0	2.28
C	3	2.8, 3.0, 3.0	2.9	2.94

Catalytic measurements

The catalytic measurements resulted in a plot of the H_2-flow against time (see Figure 5.12 for RhAA/CNF(17, BH)). This curve was integrated to get an H_2-uptake pattern, which, in turn, was used to calculate the normalised initial activity (i.e., the activity at t = 0). The results are summarised in Table 5.6. Both RhAA/CNF(17) and RhAA/CNF(5) do not display any hydrogenation activity. The catalyst reduced with $NaBH_4$, on the other hand, is highly active. The activity of RhAA/CNF(17, BH) amounts to 1.1 mole H_2/g_{cat}*h. RhAA/CNF(17, DMF) shows an intermediate activity of 0.3 mole H_2/g_{cat}*h.

5.4 Discussion

Infrared spectroscopy

The appearance of the aromatic C-H bending vibration of anthranilic acid at 746 cm^{-1} and the strong decrease in intensity of the C=O stretching band at 1724 cm^{-1} in the infrared spectrum of CNF-AA strongly indicate that anthranilic acid has been bonded to the carboxyl groups of the oxidised carbon nanofibres via an amide linkage. Reaction of anthranilic acid via the carboxyl group is highly unlikely, because an acyclic acid anhydride, which is very unstable, would be the result.[53] Unfortunately, no amide C=O stretching vibration could be observed.

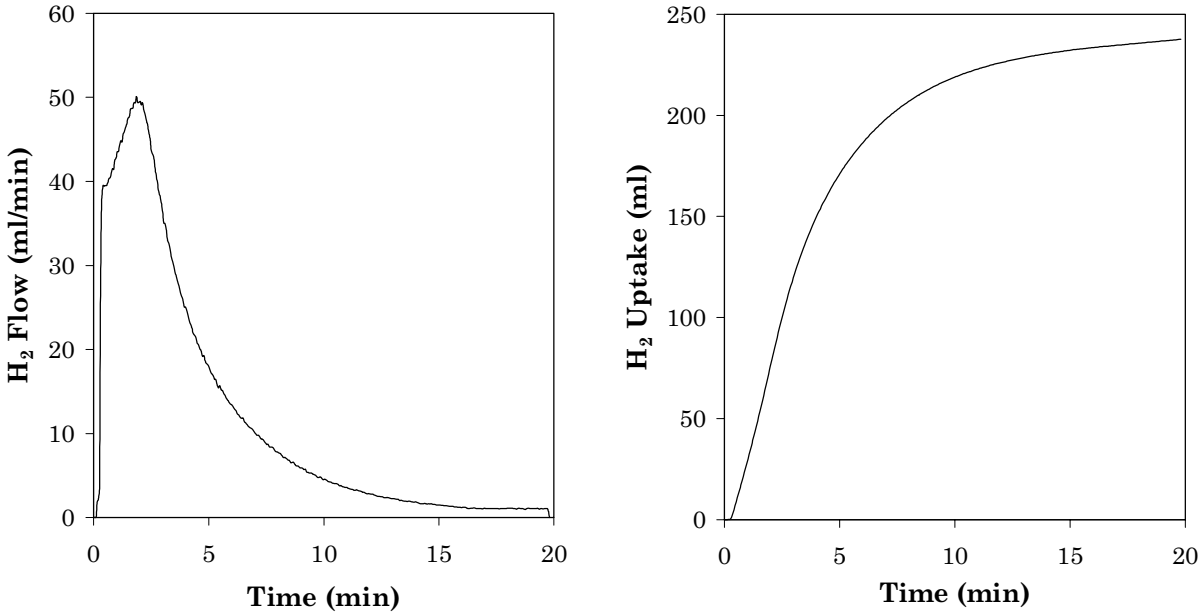

Figure 5.12 H_2-flow and H_2-uptake curves of RhAA/CNF(17, BH).

Table 5.6 Initial activities for the different catalysts.

Catalyst	Initial activity (mole H_2/g_{cat}*h)
RhAA/CNF(17)	0.0
RhAA/CNF(5)	0.0
RhAA/CNF(17, BH)	1.1
RhAA/CNF(17, DMF)	0.3

This band would be expected to be situated at about 1650 cm^{-1}.[24, 26, 27, 51] In this region the adsorbed water peak and bands originating from anthranilic acid occur as well and, therefore, no clear statement concerning the presence or absence of this vibration can be made.

The IR spectrum of CNF-$SOCl_2$ is identical to that of oxidised fibres. No evidence for acid chloride groups could be found. However, it is possible that the acid chloride groups are not stable and that they are converted back to carboxylic acid groups during IR sample preparation under the influence of water vapour in the air. Another explanation could be that anthranilic acid reacts directly with the carboxyl groups of the CNFs under the conditions used (usage of pure molten AA). To investigate this, oxidised carbon nanofibres were reacted with pure

molten anthranilic acid without prior treatment with $SOCl_2$. The infrared spectrum of these CNFs is very similar to that of CNF-AA. In other words, the anthranilic acid 746 cm^{-1} band is clearly visible and the 1724 cm^{-1} C=O stretching vibration of the carboxyl group has almost disappeared. This result makes clear that anthranilic acid can react directly with the CNF carboxyl groups. This reaction was also investigated by Pittman *et al.*, [54] who reacted PAN carbon fibres oxidised with HNO_3 with tetraethylenepentamine at 190°C. In conclusion, water-sensitive acid chloride groups may be formed on the surface of the CNFs, but their formation is not necessary to achieve the bonding of AA to carbon nanofibers.

X-ray photoelectron spectroscopy

The N_{1s} XPS spectra show the appearance of nitrogen on the surface of the CNFs after reaction with anthranilic acid. This nitrogen is not removed by any of the further treatments that are done with the CNF-AA fibres (complexation of Rh, catalytic reaction and/or reduction with $NaBH_4$), indicating that it must be tightly bound to the carbon nanofibre surface. XPS also shows that, after treatment with $SOCl_2$, the fibres should be dried in vacuum for a long period of time in order to remove all DMF from the surface of the fibres. The effect of traces of DMF on the surface of the CNFs is dealt with later in this section.

The XPS Cl_{2p} results also provide valuable information about the followed immobilisation sequence. Chlorine appears on the surface of the fibres after reaction with $SOCl_2$ and disappears again after bonding of anthranilic acid. This suggests that acid chloride groups have been formed that are subsequently used for the bonding of AA. If the acid chloride groups are unstable in air, the XPS Cl signal then probably originates from HCl that is formed during the decomposition reaction. After complexation of Rh chlorine is present again, implying that this element is present near the rhodium.

XAFS spectroscopy

The outcome of the analysis of the EXAFS data of RhAA/CNF(17) demonstrates that the central rhodium atom has six nearest neighbours (typical for Rh[III]) and that one of these neighbours is a chlorine atom. Furthermore, the EXAFS fit reveals an interaction with three carbon atoms at a longer distance. The EXAFS results imply that, for reasons of charge compensation of the Rh(III), the carboxyl group as well as the nitrogen atom of the former amine group of anthranilic acid is ionised. The three carbon atoms may originate from the benzyl ring of anthranilic acid or from the carbon nanofibre support.

The EXAFS data also shed more light on the structure of the $NaBH_4$-reduced catalyst RhAA/CNF(17, BH). Because no reduction prior to the EXAFS measurement was carried out, the result of the analysis of the EXAFS data points to small rhodium particles that are partly oxidised. The particles probably have a core of rhodium metal surrounded by rhodium oxide. As an interaction of

the Rh atoms with the carbon support is also observed, it is most likely that the rhodium particle is semi-spherical. Because the rhodium particles are partially oxidised, it is not possible to directly estimate the particle size from the co-ordination number. However, the particles should be small, because an interaction with the support is still observed and the catalyst displays a high hydrogenation activity. We roughly estimate the particle size to be in between 1.5 and 2 nm.

The complex RhAA/CNF(5) contains some Rh-Rh. As this complex probably contains a mixture of different structures, a reliable interpretation of the EXAFS data cannot be given. The RhAA/CNF(17, DMF) catalyst consists of Rh particles that have an oxidised outer surface. These particles are fairly large: no interaction with the CNF support can be distinguished.

General discussion

All characterisation techniques agree very well with each other. With IR an amide bond between the carboxyl groups on the surface of the carbon nanofibres and anthranilic acid was observed, while the XPS N_{1s} region showed the presence of tightly bound nitrogen on the CNF surface after attachment of AA. Furthermore, XPS showed that the rhodium in the as-synthesised RhAA/CNF(17) complex is in the trivalent oxidation state and that after reduction with $NaBH_4$ zerovalent Rh is formed. The XANES results are fully in agreement with these observations.

Although the EXAFS data give very valuable information about the nature and amount of neighbours of Rh and their mutual distance, a structure is not easily visualised. Therefore, the molecular modelling program was used. The constructed model of RhAA/CNF(17) agrees very well with the EXAFS results. The six nearest neighbours have distances that accord with EXAFS. More importantly, the three nearest carbon atoms in the model have an average distance that matches the EXAFS distance. As one of these carbon atoms belongs to the former carboxyl group of the carbon nanofibre, this is another strong indication for the covalent bonding of the complex to the fibres. The model also shows that although the complex is closely bonded to the CNF surface and steric hindrance is expected, the Rh in the Rh-anthranilic acid complex is able to obtain a regular octahedral surrounding.

The catalytic data have shown that when the Rh in the Rh-anthranilic acid complex is in the trivalent oxidation state, no catalytic activity is observed. Only after formation of rhodium metal particles the catalyst is active in the hydrogenation of cyclohexene. It is known that Rh(I) is able to perform the oxidative addition-reductive elimination cycle that is needed for catalysis of hydrogenation reactions by metal complexes. Therefore, it was tried to reduce the Rh(III) in RhAA/CNF(17) to the univalent oxidation state by the action of $NaBH_4$. This reductor has been used before for this purpose for the polystyrene-immobilised Rh(III)-AA complex.[5] The XPS and XANES data have shown that a

large part of the rhodium in RhAA/CNF(17, BH) has become Rh(0) after reduction. Clearly, the reduction of the Rh(III) to Rh(I) cannot be achieved with $NaBH_4$. Its reducing properties are probably too strong. Therefore, the activation of the immobilised Rh-anthranilic acid complex should be executed differently. One option could be the use of a milder reductant than $NaBH_4$. Another alternative might be to introduce the rhodium already as Rh(I) and not as Rh(III). A risky reducing step would then be circumvented.

As was already shown above with XPS, treatment of the oxidised fibres with $SOCl_2$/DMF results in the presence of DMF on the fibres if the drying procedure in vacuum is carried out only for a few hours. The final complex RhAA/CNF(5) contains some Rh-Rh. Likewise, when it is attempted to use a solution of anthranilic acid in DMF for the attachment of this ligand to the fibres, this procedure leads to the formation of large Rh particles (RhAA/CNF(17, DMF). As Rh(0) is formed in both cases, we postulate that zerovalent rhodium is formed by the reducing properties of DMF. When DMF is present on the surface of the carbon nanofibres, some or all of the rhodium chloride is reduced to Rh(0). Only when DMF is totally removed, which presumably was achieved with the RhAA/CNF(17) complex after evacuation for 17 hrs, the rhodium can fully co-ordinate to anthranilic acid.

5.5 Conclusions

The immobilisation of Rh/anthranilic acid onto fishbone carbon nanofibres was executed via (i) surface oxidation of the fibres, (ii) conversion of the carboxyl groups into acid chloride groups, (iii) attachment of anthranilic acid and (iv) complexation to rhodium(III). We have shown that anthranilic acid bonds to the CNFs by an amide linkage with carboxyl groups that are present after surface oxidation of the fibres. The immobilised anthranilic acid complexes to rhodium via the nitrogen atom and the carboxyl group. The co-ordination sphere of the trivalent Rh atom is further occupied by three water molecules and a chloride ion. To our best knowledge, this is the first example of a metal-ligand complex immobilised by covalent bonding on carbon nanofibres or carbon nanotubes.

The as-synthesised complex is not active in the hydrogenation of cyclohexene. Therefore, we reduced the rhodium with sodium borohydride in order to get monovalent rhodium. Rh(I) can undergo the oxidative addition-reductive elimination cycle that is needed for catalysis. However, the reduction procedure with $NaBH_4$ results in the formation of small rhodium particles with an estimated diameter of 1.5-2 nm on the CNFs. The hydrogenation activity of these particles is very high. We conclude that another activation procedure for the immobilised Rh/anthranilic acid system, such as reduction with a milder reduction agent or complexation of the rhodium in the Rh(I) state, must be designed. Solvents with reducing properties should be used carefully during the

immobilisation sequence. We have shown that traces of DMF on the surface of the carbon nanofibres already results in the formation of some zerovalent rhodium. Usage of anthranilic acid in DMF gives rhodium metal particles as well. The formation of acid chloride groups by the action $SOCl_2$ is not necessary to bring about the bonding of anthranilic acid to the CNFs. Under the conditions used, anthranilic acid can react directly with the carboxylic groups of the fibres.

Acknowledgements

We wish to acknowledge A. Mens for the generation of the XPS spectra and dr. O. Gijzeman for the discussions concerning the XPS data. We would like to thank the HASYLAB (Hamburg, Germany) for the opportunity to perform EXAFS measurements at beamline station X1.1. We are grateful for the collection of the EXAFS data by the EXAFS measurement team.

References

1 C.U. Pittman, Jr. in Comprehensive Organometallic Chemistry (Eds. G. Wilkinson, F.G.A. Stone, and E.W. Abel), vol 8, Pergamon Press, Oxford, 1982, p. 553
2 F.R. Hartley, Supported Metal Complexes, D. Reidel publishing company, Dordrecht, 1985
3 Yu. I. Yermakov and L.N. Arzamaskova, *Stud. Surf. Sci. Catal.* **27** (1986), 459
4 A. Choplin and F. Quignard, *Coord. Chem. Rev.* **178-180** (1998), 1679
5 N.L. Holy, *Tetrahedron Lett.* **42** (1977), 3703
6 N.L. Holy, *Fundam. Res. Homogeneous Catal.* **3** (1979), 691
7 N.L. Holy, *Chemtech* (1980), 366
8 O.N. Efimov, M.L. Khidekel', V.A. Avilov, P.S. Chekrii, O.N. Eremenko, and A.G. Ovcharenko, *J. Gen. Chem. USSR (Eng. Trans.)* **38** (1968), 2581
9 V.A. Avilov, Yu. G. Borod'ko, V.B. Panov, M.L. Khidekel', and P.S. Chekrii, *Kinet. Catal. (Eng. Trans.)* **9** (1968), 582
10 O.N. Efimov, O.N. Eremenko, A.G. Ovcharenko, M.L. Khidekel', and P.S. Chekrii, *Bull. Acad. Sci. USSR, Div. Chem. Sci. (Eng. Trans.)* (1969), 778
11 V.A. Avilov, M.L. Khidekel, O.N. Eremenko, O.N. Efimov, A.G. Ovcharenko, and P.S. Chekry, *US patent* 3,755,194 (1973)
12 E.N. Frankel, J.P. Friedrich, T.R. Bessler, W.F. Kwolek, and N.L. Holy, *J. Am. Oil Chem. Soc.* 1980, 349
13 See Chapter 3 of this thesis
14 K.P. de Jong and J.W. Geus, *Catal. Rev.-Sci. Eng.* **42-4** (2000), 481
15 A.A. Keterling, A.S. Lisitsyn, V.A. Likholobov, A.A. Gall', and A.S Trachum, *Kinet. Catal. (Eng. Trans.)* **31-6** (1990), 1273

16 Yu. Yu. Volodin, A.T. Teleshev, V.V. Morozova, A.V. Tolkachev, Yu. S. Mardashev, and E.E. Nifantyev, *Russ. Chem. Bull.* **48-5** (1999), 899
17 Y. Zhang, H.-B. Zhang, G.-D. Lin, P. Chen, Y.-Z. Yuan, and K.R. Tsai, *Appl. Catal., A* **187** (1999), 213
18 H.B. Kagan, T. Yamagishi, J.C. Motte, and R. Setton, *Isr. J. Chem* **17** (1978), 274
19 M.V. McCabe and M. Orchin, *Fuel* **55** (1976), 266
20 B.F. Watkins, J.R. Behling, E. Kariv, and L.L. Miller, *J. Am. Chem. Soc.* **97-12** (1975), 3549
21 M. Fujihira, A. Tamura, and T. Osa, *Chem. Lett.* (1977), 361
22 L. Horner and W. Brich, *Liebigs Ann. Chem.* (1977), 1354
23 J.C. Lennox and R.W. Murray, *J. Am. Chem. Soc.* **100-12** (1978), 3710
24 T. Atoguchi, A. Aramata, A. Kazusaka, and M. Enyo, *J. Electroanal. Chem.* **318** (1991), 309
25 J. Liu, A.G. Rinzler, H. Dai, J.H. Hafner, R.K. Bradley, P.J. Boul, A. Lu, T. Iverson, K. Shelimov, C.B. Huffman, F. Rodriguez-Macias, Y.-S. Shon, T.R. Lee, D.T. Colbert, and R.E. Smalley, *Science* **280** (1998), 1253
26 J. Chen, M.A. Hamon, H. Hu, Y. Chen, A.M. Rao, P.C. Eklund, and R.C. Haddon, *Science* **282** (1998), 95
27 M.A. Hamon, J. Chen, H. Hu, Y. Chen, M.E. Itkis, A.M. Rao, P.C. Eklund, and R.C. Haddon, *Adv. Mater.* **11-10** (1999), 834
28 J.S. Pizey in Synthetic Reagents (Ed. J.S. Pizey), vol. 1, Ellis Horwood, Chichester, 1974, p. 321
29 M.S. Hoogenraad, PhD Thesis (1995), Utrecht University, The Netherlands
30 M.S. Hoogenraad, M.F. Onwezen, A.J. van Dillen, and J.W. Geus, *Stud. Surf. Sci. Catal.* **101** (1995), 1331
31 J.W. Geus, M.S. Hoogenraad, and A.J. van Dillen in Synthesis and Properties of Advanced Catalytic Materials (Eds. E. Iglesia, P.W. Lednor, D.A. Nagaki, and L.T. Thompson), Materials Research Society Pittsburgh, Pittsburgh, 1995, p. 87
32 W. Teunissen, PhD Thesis (2000), Utrecht University, The Netherlands
33 J.W.Geus, *Stud. Surf. Sci. Catal.* **16** (1983), 1
34 M. Vaarkamp, B.L. Mojet, F.S. Modica, J.T. Miller, and D.C. Koningsberger, *J. Phys. Chem.* **99-43** (1995), 16067
35 http://www.xsi.nl
36 M. Vaarkamp, I. Dring, R.J. Oldman, E.A. Stern, and D.C. Koningberger, *Phys. Rev. B* **50** (1994), 7872
37 J.W. Cook Jr and D.E. Sayers, *J. Appl. Phys.* **52** (1981), 5024
38 D.C. Koningsberger, B.L. Mojet, G.E. van Dorssen, and D.E. Ramaker, *Top. Catal.* **10** (2000), 143
39 R.W.G. Wyckhoff, Crystal Structures, vol. 1, 2nd Ed., John Wiley & Sons, Inc., New York, 1963, p. 10
40 J.M.D. Coey, *Acta Cryst.* **B26** (1970), 1876
41 H. Bärnighausen and B.K. Handa, *J. Less-Common Metals* **6** (1964), 226
42 D.C. Koningsberger *Jpn. J. Appl. Phys.* **32** (1993), 877.

43 M.S.P. Shaffer, X. Fan, and A.H. Windle, *Carbon* **36-11** (1998), 1603
44 W.M. Prest and R.A. Mosher in Colloids and Surfaces in Reprographic Technology (Eds. M. Hair and M. Croucher), ACS Symposium Series Vol. 200, ACS, Washington, 1982, p. 225
45 K. Nakamoto, Infrared and Raman Spectra of Inorganic and Coordination Compounds 4th edition, John Wiley, New York, 1986, p. 124
46 U. Zielke, K.J. Hüttinger, and W.P. Hoffman, *Carbon* **34-8** (1996), 983
47 P. Painter, M. Starsinic, and M. Coleman in Fourier Transform Infrared Spectroscopy, Applications to Chemical Systems (Eds. J.R. Ferraro, L.J. Basile), Vol. 4, Academic Press, Inc., Orlando, 1985, p. 169
48 D.B. Mawhinney, V. Naumenko, A. Kuznetsova, and J.T. Yates, *J. Am. Chem. Soc.* **122** (2000), 2383
49 H.P. Boehm, *Carbon* **32-5** (1994), 759
50 See Chapter 2 of this thesis
51 B.S. Furniss, A.J. Hannaford, P.W.G. Smith, and A.R. Tatchell, Vogel's textbook of practical organic chemistry, 5th Ed., Longman, London, 1989, p. 254
52 J.F. Moulder, W.F. Stickle, P.E. Sobol, and K.D. Bomben, Handbook of X-ray Photoelectron Spectroscopy, Perkin-Elmer corporation, United States, 1992, p. 117
53 M.A. Fox and J.K. Whitesell, Organic Chemistry, 2nd Ed., Jones and Bartlett Publishers, Boston, 1997, p. 629
54 C.U. Pittman, Jr., G.-R. He, B. Wu, and S.D. Gardner, *Carbon* **35-3** (1997), 317